Climate Dynamics (2005)
DOI 10.1007/s00382-005-0041-4

Martin Stendel · Irene A. Mogensen
Jens H. Christensen

Influence of various forcings on global climate in historical times using a coupled atmosphere–ocean general circulation model

Received: 15 November 2004 / Accepted: 14 May 2005

Abstract The results of a simulation of the climate of the last five centuries with a state-of-the-art coupled atmosphere–ocean general circulation model are presented. The model has been driven with most relevant forcings, both natural (solar variability, volcanic aerosol) and anthropogenic (greenhouse gases, sulphate aerosol, land-use changes). In contrast to previous GCM studies, we have taken into account the latitudinal dependence of volcanic aerosol and the changing land cover for a period covering several centuries. We find a clear signature of large volcanic eruptions in the simulated temperature record. The model is able to simulate individual extreme events such as the ''year without a summer'' 1816. Warm periods in the early seventeenth century and the second half of eighteenth century occur in periods of increased solar irradiation. Strong warming is simulated after 1850, in particular over land, going along with an increase of the positive North Atlantic Oscillation (NAO) phase. Consistent circulation anomalies are simulated in multidecadal means with similarity to observed and reconstructed anomalies, for example during the late seventeenth and early eighteenth century. The model is able to reproduce some of the observed or reconstructed regional patterns. We find that cooling around 1700 and at the end of the eighteenth century is less than in other studies, due to the relatively small variations in solar activity and the relatively modest volcanic forcing applied here. These cooling events are not restricted to Europe and North America, but cover most of the Northern Hemisphere. Colder than average conditions, for example during the late seventeenth and early eighteenth centuries, go along with a decrease in pressure difference between low and high latitudes and a decrease of the North Atlantic Oscillation. This favours positive sea ice anomalies east of Greenland and around Iceland, leading to widespread negative temperature anomalies over Europe. We also find characteristic blocking patterns over Western Europe, in particular during autumn, which contribute to the advection of cold air.

M. Stendel (✉) · I. A. Mogensen · J. H. Christensen
Danish Meteorological Institute, Lyngbyvej 100,
2100 Copenhagen, Denmark
E-mail: mas@dmi.dk
Tel.: +45-3915-7446
Fax: +45-3915-7460

1 Introduction

Considerable attention has recently been paid to the evolution of climate and in particular temperature over the last couple of centuries. Since we generally do not have a sufficient amount of direct measurements prior to about 1850, so-called proxy data (tree rings, ice cores, corals and historical documents) must be used to assess the climate of earlier times. In order to put the temperature evolution of the twentieth century into a longer-term context, estimates of natural variability (internal variations of the climate system in the absence of external forcings) as well as forced variability (both natural and anthropogenic) are required. Several such multi-century reconstructions exist and have received considerable attention, e.g. Mann et al.'s ''hockey stick'' (Mann et al. 1999). Other reconstructions have been presented, e.g. by Huang et al. (2000), Briffa et al. (2001) and Esper et al. (2002), the first based on borehole temperatures and the other two on tree rings. An extensive review paper by Jones and Mann (2004) puts these and other estimates of past temperature variability in context. Using idealised proxy records obtained from a coupled model simulation, von Storch et al. (2004) argued that centennial variability may have been larger than these empirical reconstructions indicate. A similar result was obtained by Moberg et al. (2005) who applied a wavelet transform technique to combine information from high-resolution (tree rings)

and low-resolution proxy data (ice cores, corals, sediments, boreholes).

Climate reconstructions based on proxies have inherent uncertainties (Jones and Mann 2004). The resolvable variables and the regions for which these reconstructions are derived are not necessarily identical. As an example, tree growth is sensitive to temperature and precipitation, but the actual ring thicknesses will depend on which quantity is the limiting factor. They can therefore differ considerably even for nearby locations. Furthermore, tree-ring-based climate reconstructions are generally limited to the respective warm season in the extratropics, while ice core data are restricted to the polar regions and some tropical mountains, and coral data generally come from shallow tropical and subtropical ocean regions. Since this makes a direct comparison difficult, so-called multi-proxy methods (Mann et al. 1998; Luterbacher et al. 2002, 2004) have been developed.

In such a situation, multi-century transient climate simulations can help us to gain understanding of the temperature variations of past centuries and of the underlying physical processes when conducted with state-of-the-art coupled general circulation models. Such simulations have recently been conducted either as time-slices (Shindell et al. 2001a) or as transient experiments (Cubasch et al. 1997; Hegerl et al. 1997; Cubasch and Voss 2000; Stott et al. 2000; Crowley 2000; Zorita et al. 2004). Their results agree broadly with the reconstructions of Mann et al. (1999) and other authors. According to both model results and reconstructions, there was an extended period until the mid-nineteenth century with temperatures lower than present. This period is often (somewhat incorrectly, see Jones and Mann 2004) termed the Little Ice Age (LIA). There is historical evidence for particularly low temperatures in Europe, Asia and North America during the so-called Late Maunder Minimum (LMM, circa 1675–1715; Mann et al. 1998; Luterbacher et al. 2001; Luterbacher et al. 2004), a period with reduced solar activity (Eddy 1976). However, several proxies from the Pacific region (Druffel and Griffin 1993; Quinn et al. 1998; Hendy et al. 2002) also show low temperatures during this period.

In order to conduct such a transient simulation, it is essential to be able to quantify as many of the various natural and anthropogenic forcings that are at play as realistically as possible. The work documented in this paper differs from previous publications on the same subject by two aspects: we have included a latitude dependence of volcanic aerosol and a description of land-use changes in the forcing. While most publications have used global averages of volcanic aerosol optical depth, a few studies taking into account a latitudinal dependence have been published (Stott et al. 2000; Hansen et al. 2002; Ammann et al. 2003). All of these, however, have covered only the last roughly 100 years.

Numerous attempts have been made to quantitatively assess the impact of volcanic eruptions on climate. One problem inherent to many of these reconstructions is that they rely not on volcanism-dependent, but on climate-dependent, proxies such as historical documents or tree rings. The first volcanic index, the dust veil index (DVI) was published by Lamb (1970). It consists of historical reports, optical phenomena and (for the post-Krakatoa period) radiative measurements. Since temperature changes go into the index, there is a possibility of circular reasoning when relating climate variables to the index. The volcanic explosivity index (VEI, Newhall and Self 1982) avoids these problems, since it is entirely based on volcanic data. However, there is no possibility of obtaining the height of the eruption column and therefore the "climate relevance" from the VEI.

Both DVI and VEI are global averages. There is, however, a distinct difference between tropical and high-latitude eruptions with respect to their effect on climate (see Robock 2000 for a detailed discussion). Therefore, Sato et al. (1993) created a zonally dependent time series of aerosol optical depth, which is based on optical measurements and therefore only covers the last 150 years. Information about earlier volcanic activity can be obtained by measuring the acidity in ice cores, which is due to the deposition of volcanic sulphate on glacial ice following an eruption. However, individual ice cores are quite noisy (small eruptions nearby may have the same signature as large distant eruptions), so multiple ice cores have to be used. Robock and Free (1995, 1996) constructed such an ice core volcanic index (IVI) from Greenland, Ellesmere Island and Antarctic ice cores. More recently, Robertson et al. (2001) created an annually resolved, latitude-dependent volcanic aerosol index (VAI) for the last five centuries which combines ice core data from high latitudes of both hemispheres with historical observations and satellite data. Due to the potential influence of non-volcanic aerosol (e.g. from deserts), low-latitude, high-elevation ice cores were excluded from the analysis.

Not only is the geographical position of the volcano important, but also the timing of an eruption (see Robock 2000 for discussion). This can be implicitly taken into account by an appropriate scaling factor in the Robertson et al. data set. As an example, the date of the Tambora eruption (10 and 11 April 1815) is known as well as the fact that there were no large eruptions in the previous 3 or 4 years. We can therefore assign the optical depth anomalies in 1815 due to the eruption to the last two-thirds of the year. However, there are a number of eruptions where we do not know the exact date of eruption (and sometimes not even the source volcano).

Recently, a new latitude-dependent data set with monthly resolution was published by Ammann et al. (2003). So far, this data set is the only one that tries to incorporate realistic (model) dynamics. It is based on the amount of sulphate released and assumptions about the

peak optical depth, as well as the horizontal spread of the volcanic cloud as a function of latitude and season, which is obtained with a climate model.

The other aspect is the inclusion of land-use changes. While several authors have quantified the relative contributions of natural and anthropogenic forcings on climate, most of these studies have not explicitly taken into account anthropogenic land use changes. A number of studies using reduced complexity models (Brovkin et al. 1999; Bauer et al. 2003) yielded relatively small cooling due to land-use change on the order of 0.3 K for the last millennium. As in the present study, they have used transient scenarios of land cover change for the period of interest. Several studies have used general circulation models under equilibrium conditions. Most of them agree that global temperature changes due to land-use change are very small. However, regionally there can be quite large effects on the order of 1–2 K, both warming and cooling (Betts 2001; Zhao et al. 2001; Bounoua et al. 2002). Furthermore, several authors (Chase et al. 2000, 2001; Govindasamy et al. 2001) argued that near-surface temperature anomalies due to land-use changes are of the same order or even larger than changes due to greenhouse gases and sulphate aerosol. One example of a vegetation model interactively coupled to a GCM is given by Matthews et al. (2004).

All the models used in the studies mentioned above are of intermediate complexity. In the present study, we have chosen to force a state-of-the-art coupled climate model with a transient data set of land cover changes, which is described in detail below.

The structure of the paper is as follows: Sect. 2 gives a short introduction to the model used and describes in detail the forcings that were applied and the experiment setup. The evolution of near-surface temperature is compared to observations, reconstructions and model simulations in Sect. 3. In Sect. 4, we focus on European circulation anomalies and the North Atlantic Oscillation (NAO) during the LMM. Sect. 5 discusses the oceanic response. In Sect. 6, the results and the underlying mechanisms are discussed and set in context to other simulations.

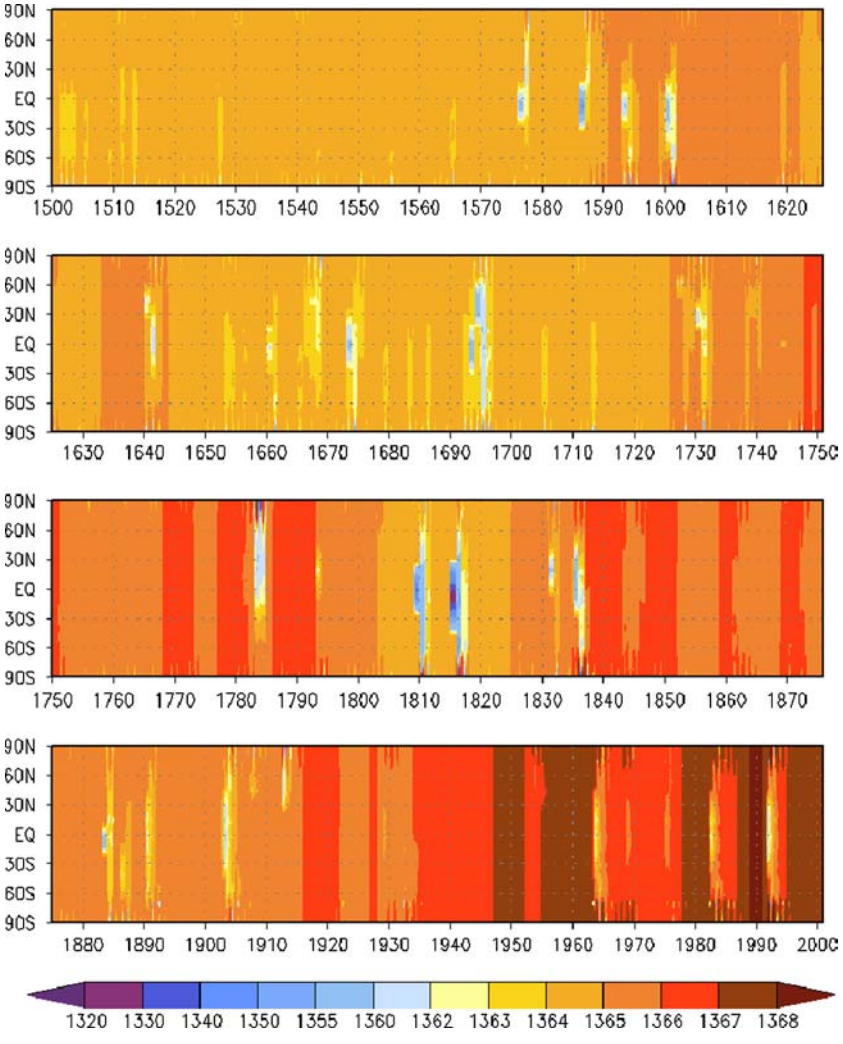

Fig. 1 Effective solar constant (W m^{-2}), expressed as the sum of solar forcing and the effect of volcanic aerosols

2 Model setup and experimental design

2.1 Model

In this study, we use the coupled ocean-atmosphere model ECHAM4-OPYC3. Its atmospheric part, ECHAM4, is described in Roeckner et al. (1999). It includes a simplified model of the tropospheric sulphur cycle (Feichter et al. 1996, 1997), which is driven by prescribed surface emissions. The direct and the first indirect aerosol effect (effect of aerosols on droplet concentration and size) are taken into account, whereas the effect on cloud lifetime is neglected. Also the effect of prescribed changes in tropospheric ozone is included, whereas the forcing due to stratospheric ozone depletion (Ramaswamy et al. 1996) is neglected. Prognostic variables (vorticity, divergence, logarithm of surface pressure, temperature, specific humidity, and mixing ratio of total cloud water) are represented by spherical harmonics with a triangular truncation at wave number 42 (T42), equivalent to a horizontal resolution of approximately 2.8°. In the vertical, 19 hybrid sigma-pressure levels are used, with the uppermost level at 10 hPa.

The ocean model is an extended version of the OPYC model (Oberhuber 1993), which consists of sub-models for the interior ocean, the surface mixed layer and sea-ice. The ocean model has 11 layers, with the horizontal resolution in the extratropics approximately corresponding to that of the atmospheric model. Near the equator, the latitudinal grid distance is gradually decreased to 0.5°.

Ocean and atmosphere are quasi-synchronously coupled, exchanging information once per day. An annual mean flux correction for freshwater and heat is applied, based on present-day climate conditions. Further details about the model can be found in Stendel et al. (2000) and references therein.

Another long transient climate simulation has recently been published by Zorita et al. (2004). While we here use the same atmospheric model as these authors, but with a higher resolution (T42 truncation instead of T30), Zorita et al.'s experiment differs from the one described here in the ocean component as well as in the forcing data used.

2.2 Forcings

Next, the individual forcings utilised in this study are described in detail. As natural forcings, solar irradiation variability and volcanic emissions are taken into account. Anthropogenic forcings include time-dependent concentrations of greenhouse gases and chlorofluorocarbons (CFCs), land-use changes and a simplified tropospheric sulphur cycle. Orbital variations can be neglected due to the comparatively short period that is investigated here (compare e.g. Lorenz and Lohmann 2004).

2.2.1 *Solar irradiation variability*

We used the data set of Lean et al. (1995, updated), covering the period 1500–2000 with annual resolution, in which hypothesised spectral changes in the ultraviolet part of the spectrum are considered. From 1610 onwards, direct observations of the 11-year solar cycle from sunspots are available. For the 110 years before, reconstructions from ^{10}Be ice core and ^{14}C tree ring data were used. A low-frequency trend with an increase of total solar irradiation by about 0.2% from the Maunder Minimum until today is visible, see Fig. 1. This trend (for discussion compare Solanki et al. 2004) was obtained from calibration with stars similar to the Sun. Beryllium is produced in the upper atmosphere and its formation is weakened by solar activity. However, the high-frequency (11 years) relation to insolation is not very strong, in particular during solar minimum periods. One can in principle use the ^{14}C record to calibrate the Beryllium data. As ^{10}Be, this carbon isotope depends on the flux of cosmic rays, which goes along with solar activity. The problem is that one first has to get rid of (known) climatic influences so that only the remainder can be attributed to solar activity. Since no independent calibration to irradiance exists, a change from the LMM to present-day conditions is estimated; however this is a quantity that is not well constrained (see Foukal et al. 2004).

Apart from volcanic activity (see below), Fig. 1 clearly shows several minima in solar irradiance, in particular the Spörer Minimum in the first part of the sixteenth century, the well-known Maunder Minimum (about 1650–1715) and the Dalton Minimum in the early nineteenth century. Since then, a general increase in irradiance is evident.

2.2.2 *Volcanic sulfur emissions*

The volcanic aerosol distribution during the last 500 years is far from well known since no direct

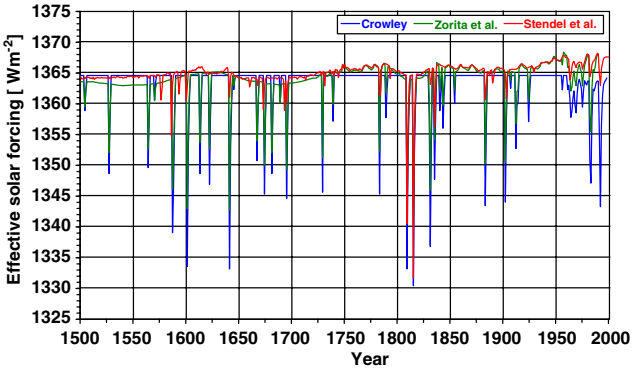

Fig. 2 Comparison of the globally averaged effective solar forcing used in Crowley et al. (2000), Zorita et al. (2004) and in this study. The volcanic optical depth used in this study consists of annually resolved data (Robertson et al. 2001) for the period 1500–1889 and monthly resolved data (Ammann et al. 2003) from 1890 onwards

observations exist. In Fig. 2, we compare the globally averaged effective solar radiation for three different data sets. Evidently, there is considerable uncertainty about the actual amount of volcanic aerosol ejected into the stratosphere, resulting in a difference by a factor of 4 between the Crowley and Robertson data sets even for reasonably well-documented eruptions like Krakatoa 1883. The Ammann et al. (2003) data set fails to describe the variations of τ for the fairly well-observed eruptions of Agung in 1963 and El Chichon in 1982 (Sato et al. 1993; Stothers 2001). This highlights the large uncertainties in reconstructing volcanic aerosol load. Here we have used the annually-resolved Robertson et al. (2001) volcanic optical depth data set for the period 1500–1889 and the monthly-resolved data of Ammann et al. (2003) from 1890 onwards.

The optical depth τ—calculated for the Robertson et al. data from the sulphate aerosol concentration in the ice following Stothers (1984) and modelled for the Ammann et al. data—can be expressed as an anomalous radiative forcing at the tropopause, following the procedure described in Andronova et al. (1999). Even though τ is only given for a single wavelength ($\lambda = 0.55$ μm), one can obtain zonally averaged estimates of the radiative forcings independently for the long wave and the solar part by taking into account monthly mean solar insolation (more specifically, the cosine of the solar zenith angle), effective emitting temperature, the fraction of daylight during a day and the planetary albedo in the absence of volcanic aerosol. The latter is obtained from the HYDE data set, which is described in detail below. Andronova et al. show that the net radiative forcing at the tropopause obtained with this approach fits well with results found using a detailed radiative transfer model. In their approach, the increase of stratospheric temperature is only estimated to obtain the long-wave forcing, but there is no feedback to the model.

We note that the forcing time series used in Zorita et al. (2004) is deduced from the Crowley data, but also assumes larger variations in solar irradiation than the data used here.

2.2.3 Well-mixed greenhouse gases

The annual concentrations of greenhouse gases (CO_2, CH_4 and N_2O) are also taken from Robertson et al. (2001). They have been obtained from ice core data. For the well-mixed carbon dioxide, one measurement from Law Dome (Antarctica) is sufficient. For methane, which is less well mixed, time series from both hemispheres have been averaged. N_2O, on the other hand, is rather variable in different measurements; therefore an average of a number of Antarctic records was used. The concentrations of CFCs have been taken from observations described in the third IPCC assessment report (Nakicenovic et al. 2000).

2.2.4 Land-use changes

In contrast to previous studies (e.g. Zorita et al. 2004), we also take into account the effects of anthropogenic vegetation changes. Land cover changes affect the climate by impacting the surface energy and moisture fluxes. We use the so-called HYDE "A" data set (Klein Goldewijk 2001), which includes on a 0.5° by 0.5° grid croplands as well as areas used as pasture, which are estimated from population densities as well as estimates of livestock, gross domestic product and industrial production. As far as possible, the data have been organized on a country level. There is one vegetation class considered to be representative for every grid cell. In a first step, the vegetation classes were assigned to the ECHAM vegetation classes (Claussen 1994 with later updates by Hagemann et al. 1999) and interpolated to the model grid. Then, following Hagemann et al., differences from present-day conditions for background albedo, forest and vegetation ratio, leaf area index and surface roughness are determined. The data set has a resolution of 50 years from 1700 to 1950, and present-day conditions are given as values for 1990. For years not included in the data set, we interpolate the fields linearly in time. Prior to 1700 and after 1990, the values have been set to those for 1700 and 1990, respectively. The data set shows large-scale deforestation in Europe in the eighteenth century, in the western U.S. in the second half of the nineteenth century and, more recently in East Asia (not shown). Historic albedos from this data set are also used for the estimation of the shortwave volcanic forcing that is described in Volcanic sulphur emissions.

2.2.5 Anthropogenic sulphate aerosol

ECHAM4 has a simplified tropospheric sulphur cycle described in detail in Roeckner et al. (1999). Sulphur emissions with their actual geographical positions are given as decadal means from 1860 onwards. The transformation to sulphate semi-Lagrangian transport of the sulphate aerosols as well as dry and wet deposition of sulphate particles from the atmosphere (Feichter et al. 1996) are taken into account. The indirect aerosol effect on cloud albedo, following Boucher and Lohmann (1995) and Lohmann and Feichter (1997), is also included. In addition, the tropospheric ozone concentration is allowed to vary as a result of prescribed concentrations of anthropogenic precursor gases (CH_4, NO_x, CO) and stratospheric O_3 and NO_x whose concentrations are given for 1860 and 1985 and linearly interpolated in between (Roelofs and Lelieveld 1995).

2.3 Experiment setup

The model was run to near equilibrium conditions from present-day to A.D. 1500 conditions by applying

the pre-industrial values of all the forcings described above. After a period of 500 years, the model variables had asymptotically approached near constant values with a residual decadal surface temperature trend of -1.5×10^{-3} K and a residual decadal surface salinity trend of -2×10^{-4} psu. We note that this procedure only brings the upper 1–2 km of the ocean into approximate equilibrium; for the deep ocean, a much longer period would be needed. From this starting point, an unforced control simulation and a forced experiment including all forcings have been run for 500 years each. For an estimation of the effect of land-use changes, an additional simulation was run for the last 300 years using constant vegetation for 1700.

The forcings were applied in the following way. Land-use variables were interpolated in space and time to the ECHAM grid and then used to replace the standard model values for background albedo and related quantities. For the volcanic aerosols, the procedure following Andronova et al. (1999) was adopted, which allows for an estimate of the short- and long-wave contributions to the forcing anomalies at the tropopause as a function of optical thickness. The so obtained net forcing was then added to the solar irradiation data to form the (latitude-dependent) ''effective solar constant'' which is shown in Fig. 1. The other forcings were applied the usual way, described in Roeckner et al. (1999).

3 Evolution of near-surface temperature and comparison to proxy data

Figure 3 compares the simulated evolution of global near-surface temperature with reconstructions from instrumental observations, an energy balance model (Crowley 2000), dendrochronologies (Esper et al. 2002), borehole data (Huang et al. 2000), Mann and Jones multi-proxy reconstruction (Mann and Jones 2003) and Zorita et al.'s model simulation with the same atmospheric model in coarser resolution (Zorita et al. 2004), but with a different ocean model. Temperatures in our study generally follow the proxy data, with negative anomalies during the LMM (late seventeenth and early eighteenth century) and around 1830 as well as a strong temperature increase since the mid-nineteenth century. Over land, the overall temperature increase is 1.8°C, of which 1.5°C occurs during the twentieth century. Over the oceans, we find an increase of 1.0°C, most of which occurs during the twentieth century as well. Compared to the simulation by Zorita et al., the negative anomalies in our simulation are smaller. This can be explained by the much larger solar variability and volcanic forcing that has been used in their data set.

The temperature increase is not uniform, neither in latitude nor in time. In particular, large volcanic eruptions can influence global temperature on a time

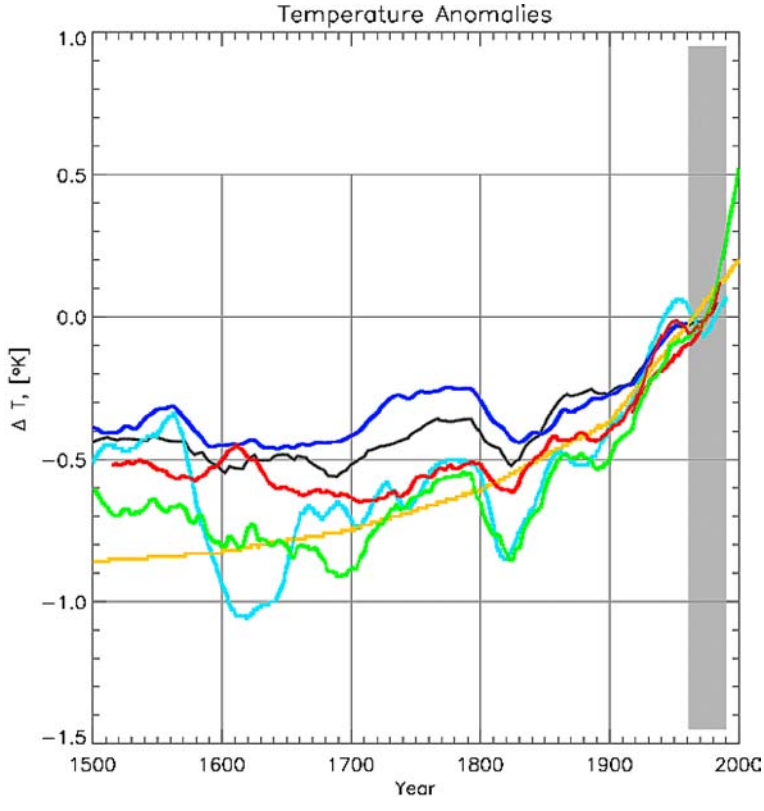

Fig. 3 Thirty-year running averages of near surface temperature anomalies 1500–2000 for the instrumental record (brown curve), the reconstructions of Huang et al. (2000, yellow curve), Esper et al. (2002, light blue) and Mann and Jones (2003, dark blue), the model simulations of Crowley (2000, black) and Zorita et al. (2004, green) and for this study (red curve)

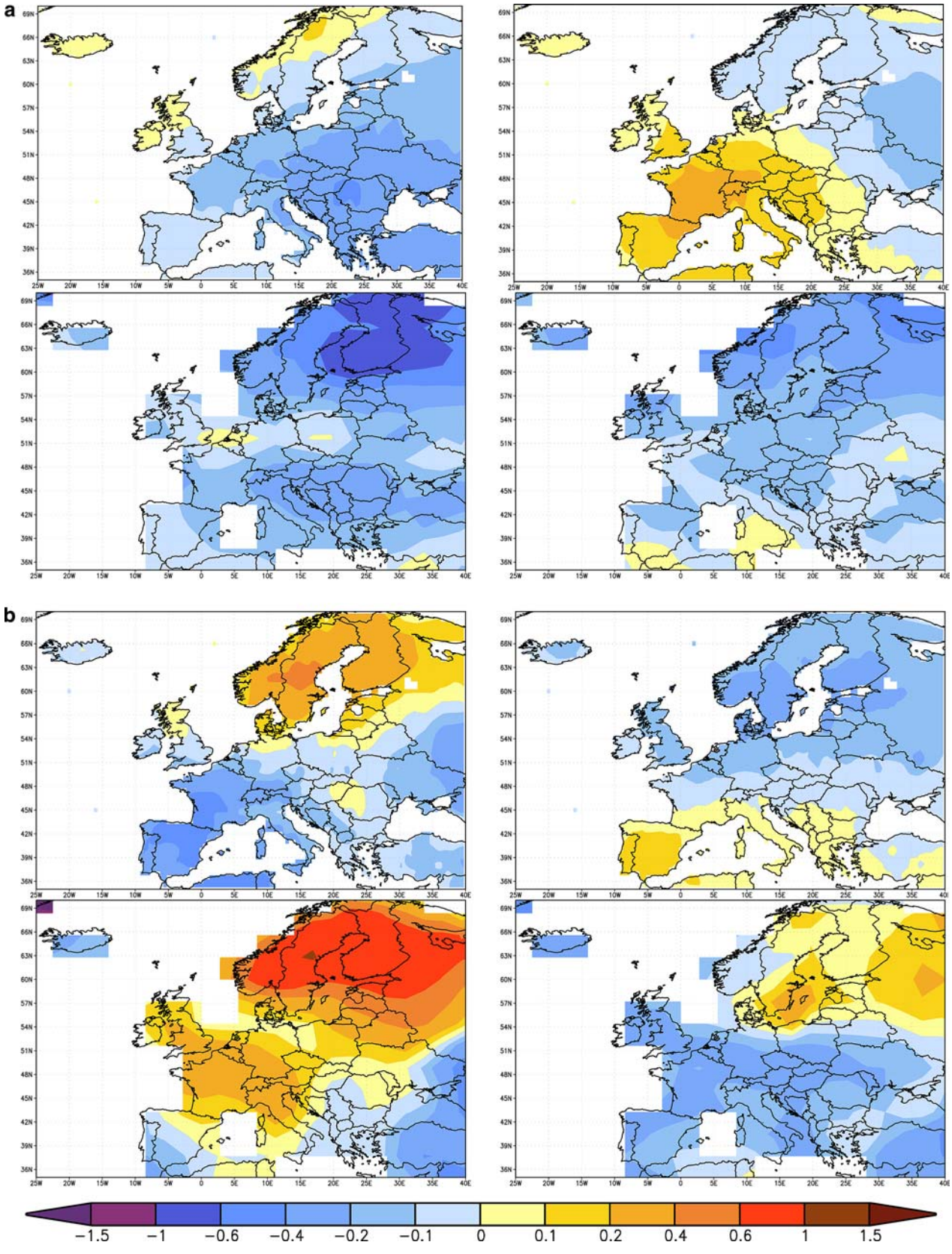

Fig. 4 Late Maunder Minimum winter (DJF, *left column*) and summer (JJA, *right column*) temperature anomalies (K) from the average 1500–1700 for (**a**) 1666–1690, (**b**) 1691–1715. *Top panels*: empirical reconstructions (Luterbacher et al. 2004), *bottom panels*: this study

scale of several years. The most striking example follows the eruption of Tambora in 1815. The "year without a summer" 1816 following this event (see e.g. Harington 1992 or Robock 1994 for extensive reviews) is evident in the simulation (not shown). Over land, the temperature decrease after the Tambora eruption amounts to more than half a degree, which is in line with estimates from historical evidence by Stothers (1984), see also Self et al. (2004). Other examples of major volcanic events leaving an imprint in the global temperature curve include Laki on Iceland in 1783 and Krakatoa (Indonesia) in 1883. Also the "1809 event" (clearly visible in ice cores, the responsible volcano remaining unknown, see Budner and Cole-Dai 2003) can be identified.

While the model is able to depict the direct radiative effects of large volcanic eruptions, it fails to simulate the flow anomalies triggered by tropical eruptions (Robock and Mao 1995; Shindell et al. 2001b) which warm the sub-polar stratosphere, thus causing an increase in the pole–midlatitude temperature gradient and therefore leading to warmer than normal temperatures in the winter following such an eruption in large parts of Europe. As mentioned above, this can be explained by the lack of feedback of the increased stratospheric temperature to the model. We also note several cooling periods on multidecadal time scales, which will be discussed in detail in the next section. Warm periods in the early seventeenth century and in the second half of the eighteenth century are likely caused by increased solar irradiation.

To assess the regional distribution of anomalies during the late seventeenth and early eighteenth century, we compare simulated and reconstructed seasonal temperature anomalies over Europe from the 200 year average 1500–1700 (Fig. 4). The temperature reconstruction is by Luterbacher et al. (2004) who used a multi-proxy approach including long instrumental time series, temperature and sea ice indices estimated from documentary proxy evidence (e.g. Pfister 1999; Glaser 2001; Xoplaki et al. 2001; Vinther et al. 2003; Bràzdil et al. 2005 and references therein) as well as a few seasonally resolved natural proxies from tree rings and Greenland ice cores. According to this reconstruction, the period was characterised by colder than average winter conditions over most of the continent and positive anomalies over most of Scandinavia. The model is able to depict this general pattern and thus seems to have skill to simulate large scale regional climate changes. For spring (not shown), the model is also able to pick up the general anomaly pattern, while simulated cold anomalies in summer extend too far south. The general increase of blocking situations over the European–Atlantic region (qualitatively defined here by positive geopotential anomalies between 40°N and 60°N and negative anomalies further south in monthly mean values) during this period (compare Luterbacher 2001; Luterbacher et al. 2001) is also simulated. We note that a thorough definition of "blocking" requires an assessment of persistence that can only be obtained from daily data (e.g., Tibaldi et al. 1994). Such an investigation is beyond the scope of this study and will be presented in a follow-up paper. In autumn we find an anomalous blocking pattern over the British Isles, whereas in the reconstructions higher than average pressure is rather found over northern Scandinavia (not shown). Accordingly, too large positive anomalies are simulated over western Europe with respect to the reconstruction, whereas the cold anomalies further east are well captured.

To assess the effect of vegetation changes, we have conducted a sensitivity experiment where background albedo, forest and vegetation ratio, leaf area index and surface roughness were held constant at 1700 values (not shown). While the global effect of vegetation changes is small (less than 0.1 K), differences up to −0.3 K are simulated over Europe in the eighteenth century and over the U.S. Great Plains in the nineteenth century with the full forcing simulation being colder. There is also a modest reduction in temperature over south eastern Asia in the first half of the 20th century. This is in agreement with estimates from transient experiments by Bertrand et al. (2002) and Matthews et al. (2003), but smaller than the results reported by Matthews et al. (2004) using an interactively coupled vegetation model.

4 Atlantic–European circulation patterns

4.1 Multidecadal circulation anomalies

In order to further assess typical Atlantic–European circulation anomalies in the model, a time series of European temperature anomalies was constructed, covering the same area as the Luterbacher et al. data. From this time series, several 25 year segments were chosen: a particularly cold period centred on 1788, a warm spell centred on 1612 and two periods covering the onset (1666–1690) and the end (1691–1715) of the cold period during the LMM. For these periods, temperature (both near-surface and deep-soil), precipitation, sea ice cover and 500 hPa height (sea level pressure is very similar) were compared to the average 1500–1700. As an example, we here show these fields for spring and autumn of the second cold period (Fig. 5). In the other seasons, anomalies are not as clearly visible, as discussed below.

During cold periods in winter (DJF), positive sea ice anomalies are found in the Greenlandic/Icelandic region. The opposite is true for warm periods. An investigation of global temperature anomalies reveals that the anomalous ice cover not only influences the temperature of adjacent regions, but also is correlated to circulation and temperature anomalies quite far away. Over Eurasia, we find a general weakening of the zonal circulation by either anomalous high pressure in the polar region ("low index" type, 1666–1690) or anomalous low pressure over most of Eurasia ("high index" type, 1776–1800). Both types of circulation anomalies favour posi-

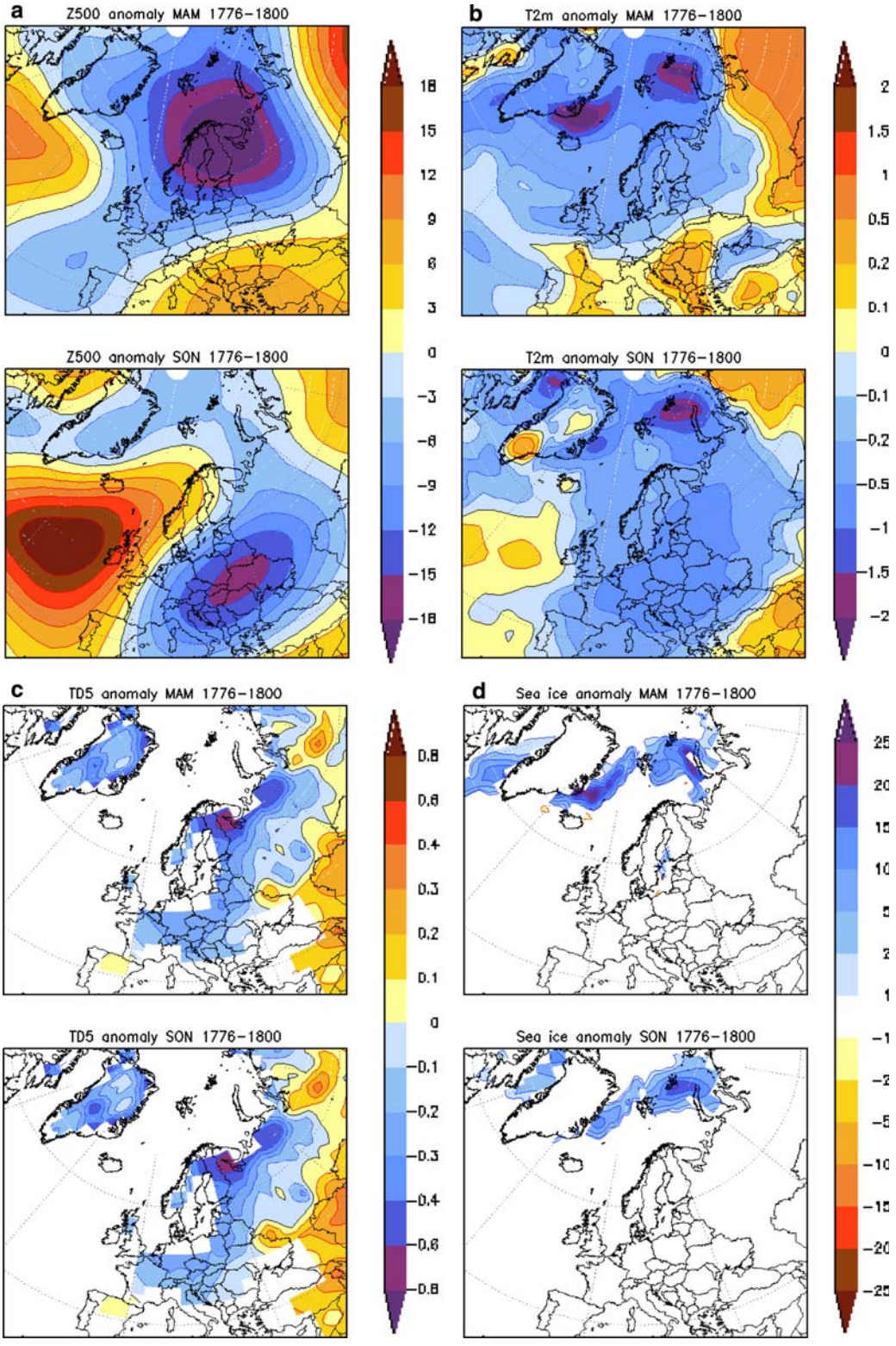

Fig. 5 Twenty-five-year (1776–1800) anomalies from the 200 year mean 1500–1700 for (**a**) 500 hPa geopotential (gpm), (**b**) 2 m temperature (K), (**c**) deep-soil temperature (K) and (**d**) sea ice cover (%). *Top panel*: spring (MAM), *bottom panel*: autumn (SON)

tive sea ice anomalies near Iceland and along Greenland's east coast. These go along with large cold anomalies both for near-surface and deep-soil temperature over Northeast Europe (Fig. 5b, c). In contrast, during both warm periods anomalous high pressure is simulated over large parts of Eurasia, favouring negative sea ice anomalies around Greenland and Iceland and increased cyclonic activity along 40°N. Anomalies that

characterised a particular winter tend to extend into the following spring.

Also in summer (JJA), cold periods are characterised by a simulated weakening of the zonal circulation caused by either anomalous high pressure over Greenland (''low index'' type, 1776–1800) or anomalous low pressure over most of Europe/Asia (''high index'' type, 1666–1690). Both circulation patterns go along with a southwest displacement (and probably weakening) of the Azores high and generally tend to transport cool Atlantic air masses into most of Europe. The opposite is the case during the periods of warm anomalies. As mentioned above, the most striking circulation anomalies occur in autumn (SON) where, even in the 25 year average, a 500 hPa anomaly of more than 20 geopotential metres is simulated over Western Europe.

4.2 The North Atlantic Oscillation

The effect of atmospheric circulation changes on temperatures in Europe is further analysed by looking at the temporal evolution of the NAO. Figure 6 shows the principal component (PC) time series of the two leading empirical orthogonal functions (EOFs) of European–Atlantic sea level pressure. The first EOF, representing the NAO, explains 37% of the total variance. Even though proxy-based NAO reconstructions exhibit only limited skill (Schmutz et al. 2000), there is evidence from reconstructions by Luterbacher et al. (2002) and Glück and Stockton (2001) for a strong increase in zonality since the mid-nineteenth century. Such an increase for the last 150 years—with the notable exception of the 1940s that were characterised by low NAO indices in the European–Atlantic region—is also visible in the model data.

Corroborating results by Zorita et al. (2004)—obtained with quite a different forcing—we find a shift of the NAO index from negative to positive values approximately halfway through the cold period during the LMM (Fig. 4). The onset phase (1666–1690) occurred with several extremely cold winters, e.g. 1683/1684, the coldest winter of Manley's (1974) Central England temperature series. This cold period is well

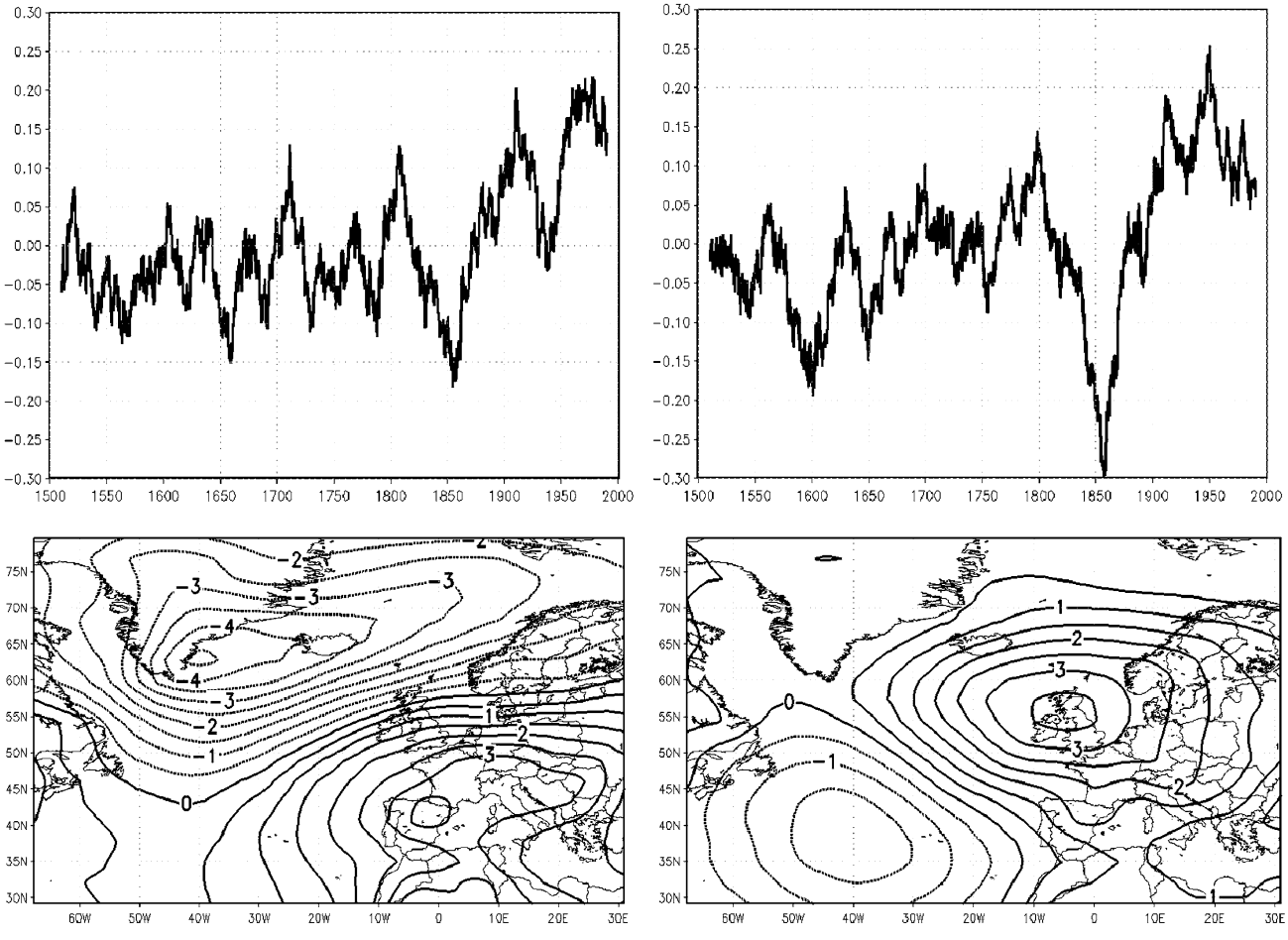

Fig. 6 Twenty-year running average of the first and second principal components (PCs, *top*) of sea level pressure in the Atlantic–European sector. The associated empirical orthogonal functions (EOFs) explain 37.0% and 19.6% of the variance, respectively. The time series have been normalised so that the information about the strength of the variation is contained in the patterns. The unit of the EOFs is hPa

covered by the model with negative anomalies near 1 K over northern Fennoscandia. The following two and a half decades (1691–1715) are generally dominated by the positive NAO phase, leading to advection of warm air into Scandinavia. The spatial structure is comparable for reconstructions and simulations. The amplitude is overestimated by the model by a factor of 2. The model is, however, not doing so well for the other seasons. While the magnitude of the anomalies is captured well, the regional distribution is not, in particular in spring and autumn. This is probably related to the comparably large number of blockings, which are not always simulated well by the model.

A circulation pattern with high pressure over the British Isles is given by EOF2, which explains almost a fifth of the variance. The corresponding PC has a large loading during most of the late seventeenth and early eighteenth century (Fig. 6), thus corroborating our findings about the increase of blocking patterns discussed above.

Part of the internal variability of the NAO may be unrelated to the applied forcings. An ensemble of experiments would therefore be desirable for a thorough assessment.

5 Oceanic response

Rahmstorf and Ganopolsky (1999) report of a general slowing down of the Atlantic thermohaline circulation (THC) under global warming conditions, caused by the decrease of surface water density by either increased warming or an anomalous freshwater flux. However, in ECHAM4/OPYC, we do not find a particular sensitivity to changes in the forcing (not shown). This is a particular property of this model: under warming conditions, the stability of the THC is caused by a poleward transport of anomalously saline water (caused by anomalous evaporation) from the tropical Atlantic. This remote effect is able to compensate for the local effects in the North Atlantic which tend to decrease the density of surface water through warming and increase in freshwater flux (Latif et al. 2000). The opposite is true for cooling conditions. Therefore, the THC remains rather stable throughout the simulation. For this particular experiment, the mean overturning is 21.0 Sv with a standard deviation of 3.2 Sv. Over the simulation period, we find a slight decrease of 0.03 Sv.

As an example for intermediate depths (below the mixed layer down to about 1,000 m), we present time series for temperature and salinity at 200 m depth in Fig. 7. The temperature curve shows a decrease for the first 200 years of the simulation, and the lowest values are found around 1700, followed by a modest increase and low temperatures a couple of years after the eruption of Tambora. From the mid-19th century, temperatures at this level increase by almost half a degree. The salinity shows a slow decrease by approximately 0.03 psu.

The vertical distribution of temperature trends in the forced simulation and in the control run is shown in Fig. 8. As mentioned before, it can be seen that even after 500 years, the deep ocean has not yet reached equilibrium. However, this does not affect the ocean layers above, at least not for the time periods considered here. Both simulations are quite similar below about 800 m. Above that depth, we see the dominating effect of the recent warming in the forced simulation whereas there is a general decrease of temperature in the control run.

6 Discussion

Near-surface temperatures as well as deep soil temperatures well below the long-term average are simulated for extended periods, including the cold period during the LMM. We find an accompanying decrease in solar irradiation and an increase in volcanic activity during the same periods. Compared to other models (Fig. 3),

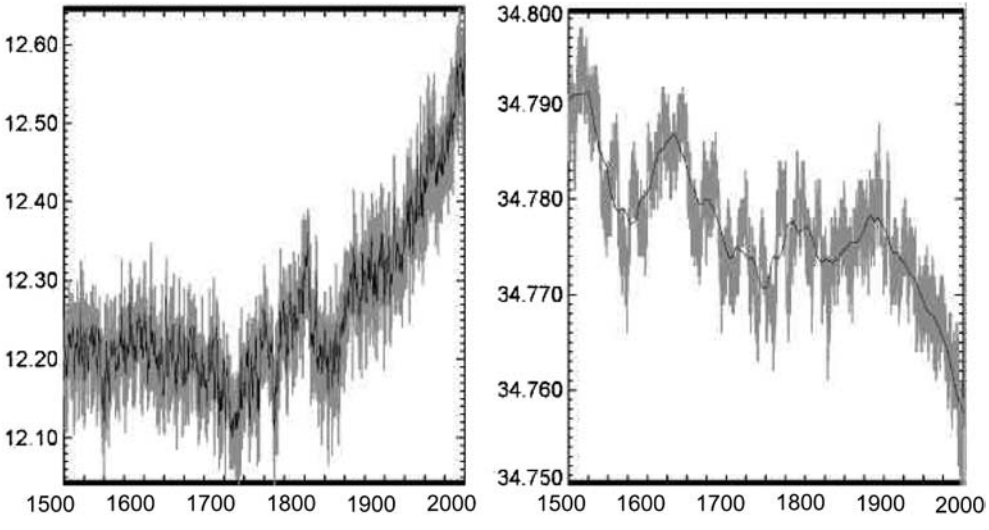

Fig. 7 Time series of temperature (°C) (*left panel*) and salinity (psu) (*right panel*) at 200 m depth in the forced simulation

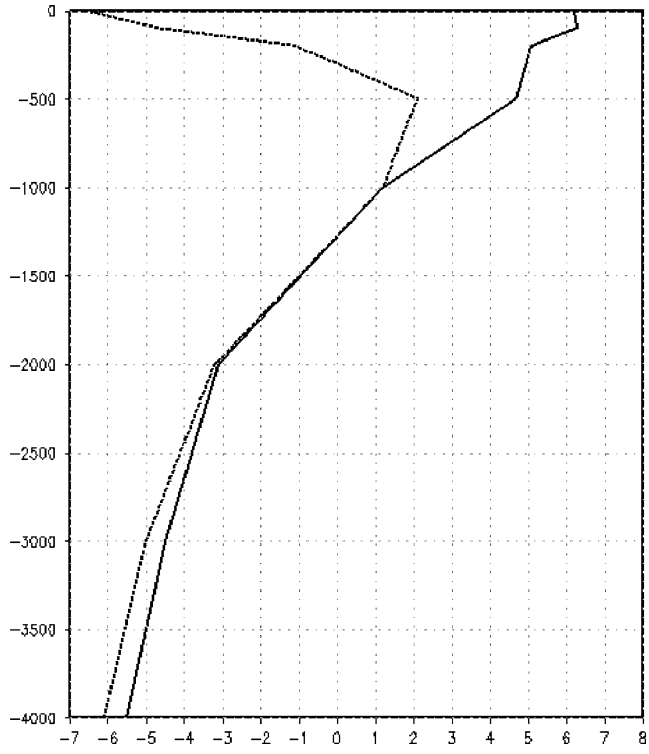

Fig. 8 Vertical cross-section of temperature trends (10^{-3} K/decade) in the forced simulation (*solid line*) and the control simulation (*dashed line*)

the model response is larger than in Crowley's (2000) energy balance model, but clearly smaller than in the simulation of Zorita et al. (2004). ECHAM4/OPYC has an effective climate sensitivity (i.e. equilibrium temperature change for CO_2 doubling) of 2.6 K, which is about the average of all IPCC models (IPCC 2001). Zorita et al.'s model, based on the same atmospheric component, has a similar sensitivity. The reason for the difference is that Crowley's model is an energy balance model, which cannot take into account nonlinear dynamic effects, in particular at high latitudes: under warming conditions for the twenty-first century, ECHAM's temperature rise is up to three times as large as in the global average (Stendel et al. 2000).

On the other hand, Fig. 2 shows that the volcanic forcing in Zorita et al.'s simulation is roughly a factor of 4 larger than in this study, with the exception of the 1809 event and the 1815 eruption of Tambora (which have comparable sizes in both experiments). Also, the multidecadal variability in solar irradiation is considerably larger in their data set. Zorita et al. assume an increase in irradiance by 0.3% from the LMM to present-day conditions (we use Robertson et al.'s 0.19%). Other authors suggest values from 0.15% (Solanki et al. 2004) to 0.65% (see discussion in Bard et al. 2000). This highlights the considerable uncertainty in solar irradiance reconstructions. The fact that there is a clear response also in our simulation can be explained by the large impact of extratropical volcanoes on high-latitude temperatures (see e.g. Laki on Iceland in 1784) in the solar part of the spectrum (see Sect. 2). Latitudinal resolution (as well as correct placement in time) of the volcanic aerosol is therefore essential, but unfortunately these quantities are generally not well known.

As suggested by Shindell et al. (2001a), a decrease in radiative forcing, caused by volcanic aerosol or a decrease in solar irradiation, leads to a decrease in the upper tropospheric temperature gradient between the tropics and high latitudes and a decreased northward transport of momentum and therefore to a weakening of the NAO. Despite the rather simplified representation of the stratosphere in ECHAM, we see a similar weakening of the zonal flow with decreased radiative forcing (not shown) in our simulation: for the 40-year average 1661–1700, the pressure difference between the Azores and Iceland is 2.1 hPa smaller than for the period 100 years later, in good agreement with the value −1.9 hPa as reported by Shindell et al. (2001a). The decrease in upper ocean temperature (Fig. 7) and a combination of decreased irradiation and high-latitude volcanic forcing may contribute to positive sea ice anomalies east of Greenland and around Iceland, regions that are particularly sensitive to circulation changes in ECHAM (Stendel et al. 2000), but probably also in reality, since there is historical evidence (e.g., Lamb 1982) for above average ice conditions around Iceland around the turn to the eighteenth century. Once such a cold anomaly has evolved, it may persist for quite some time: González-Rouco et al. (2003) show that deep soil temperatures generally follow surface air temperatures on interannual and longer timescales; on the other hand, air temperatures may be influenced from the lower boundary (compare Cox et al. 1999) by widespread below average soil temperatures (Fig. 5c). In sub-Arctic regions, the effect may be further enhanced by nonlinear effects such as freezing of previously unfrozen ground in the transition zone to permafrost.

Such a quasipersistent weakening of the zonal circulation could, on average, persist for several years and lead to cold conditions in Europe except in summer, where the thawing of the upper layer acts as a blocker from the deeper frozen soils. It would also go along with an increase of blocking situations. It remains to be examined if there is a dependence on resolution, since the remarkable increase in blockings is not apparent in the coarser resolution (T30) in Zorita et al.'s simulation. In contrast to the mechanisms discussed above, the weakening of the ocean gyre circulation, as described in Zorita et al. (2004), does not seem to play a prominent role for the present model, as the local freshening in the northern oceans is compensated by the transport of saline waters from the tropics.

7 Conclusion

We have conducted a model reconstruction of past climates, including most forcings, both natural and

anthropogenic, which differs in several aspects from comparable simulations documented so far. Tropical and high-latitude volcanoes differ distinctly in their climate effects. It is therefore important to account for the geographical position of the volcano as well as for the date of eruption, as long as it is known. Accounting for both the solar and long-wave contributions from volcanic aerosol has a large impact in high latitudes and locally enhances the effect of comparably small eruptions, such as Laki on Iceland. The effect of changing vegetation is small in the global average, but locally of comparable magnitude to the other forcings.

The level of externally forced variability in our simulation is larger than in Crowley's (2000) energy balance model. It is also larger than several reconstructions suggested, in particular that of Mann and Jones (2003). Qualitatively, it fits best the tree ring based reconstruction by Esper et al. (2002), at least for the last 300 years. In our reconstruction, the cold period during the LMM is the coldest period of the past 500 years, which is also true for the Zorita et al. simulation with much larger forcing than used here. This implies that state-of-the-art climate models are able to simulate multidecadal circulation anomalies, even under conservative forcing assumptions. In view of past climate evolution, the warm conditions at the end of the twentieth century are highly unusual and unprecedented for at least the last five centuries.

In comparison to high-resolution empirical climate reconstructions, the model, to some extent, is able to simulate regional climate anomalies, mainly in winter (DJF). As can be seen in years following large volcanic eruptions, it mainly reacts to the reduced insolation, but fails to reproduce the dynamical effects following such forcing anomalies.

Acknowledgements The empirical reconstruction of European temperatures was provided by Jürg Luterbacher. The historical land-use change data were obtained through the National Institute for Public Health and the Environment (RIVM) of The Netherlands. We would like to thank Caspar M. Ammann, Michael E. Mann, Eduardo Zorita and Hans von Storch for comments and suggestions, Torben Schmith for help with processing the OPYC data and two anonymous reviewers for valuable comments that helped to improve the manuscript. This work was funded by the EU 5th Framework project GLIMPSE (Global implications of Arctic climate processes and feedbacks) under contract EVK2-CT-2002-00164.

References

Ammann CM, Meehl GA, Washington WM, Zender CA (2003) A monthly and latitudinally varying volcanic forcing data set in simulations of 20th century climate. Geophys Res Lett 30. DOI 10.1029/2003GL016875

Andronova NG, Rozanov EV, Yang F, Schlesinger ME, Stenchikov GL (1999) Radiative forcing by volcanic aerosol from 1850 to 1994. J Geophys Res 104:16807–16826

Bauer E, Claussen M, Brovkin V, Huenerbein A (2003) Assessing climate forcings of the Earth system for the past millennium. Geophys Res Lett 30. DOI 10.1029/2002GL016639

Bard E, Raisbeck G, Yiou F, Jouzel J (2000) Solar irradiance during the last 1200 years based on cosmogenic nuclides. Tellus 52:985–992

Bertrand C, Loutre MF, Crucifix M, Berger A (2002) Climate of the last millennium: a sensitivity study. Tellus 54A:221–244

Betts RA (2001) Biogeophysical impacts of land use on present-day climate: near surface temperature and radiative forcing. Atm Sci Lett 1, DOI 10.1006/asle.2001.0023

Boucher O, Lohmann U (1995) The sulfate-CCN-cloud albedo effect: a sensitivity study with two general circulation models. Tellus B47:281–300

Bounoua L, de Fries R, Collatz G, Sellers P, Khan H (2002) Effects of land cover conversion on surface climate. Clim Change 52:29–64

Brázdil R, Pfister C, Wanner H, von Storch H, Luterbacher J (2005) Historical climatology in Europe—the state of the art. Clim Change (in press)

Briffa KR, Osborn TJ, Schweingruber FH, Harris IC, Jones PD, Shiyatov SG, Vaganov EA (2001) Low-frequency temperature variations from a northern tree ring density network. J Geophys Res 106:2929–2942

Brovkin V, Ganopolsky A, Claussen M, Kubatzki C, Pethoukov V (1999) Modelling climate response to historical land cover change. Glob Ecol Biogeogr 8:509–517

Budner D, Cole-Dai J (2003) The number and magnitude of large volcanic eruptions between 904 and 1865 AD: Quantitative evidence for a new South Pole ice core. In: Volcanism and the Earth's atmosphere. Geophys Monogr 139, American Geophysical Union

Chase T, Pielke R, Kittel T, Nemani R, Running S (2000) Simulated impact of historical land cover changes on global climate in northern winter. Climate Dynam 16:93–105

Chase T, Pielke R, Kittel T, Zhao M, Pitman A, Running S, Nemani R (2001) Relative climatic effect of landcover change and elevated carbon dioxide combined with aerosols: a comparison of model results and observations. J Geophys Res 106:31685–31691

Claussen M, Lohmann U, Roeckner E, Schulzweida U (1994) A global data set of land-surface parameters. MPI Report 135, Max-Planck-Institut für Meteorologie, Hamburg

Cox PM, Betts RA, Bunton CB, Essery RLH, Rowntree PR, Smith J (1999) The impact of new land surface physics on the GCM simulation of climate and climate sensitivity. Climate Dynam 15:183–203

Crowley TJ (2000) Causes of climate change over the last 2000 years. Science 289:270–277

Cubasch U, Voss R (2000) The influence of total solar irradiance on climate. Space Sci Rev 94:185–198

Cubasch U, Hegerl GC, Voss R, Waszkewitz J, Crowley TC (1997) Simulation with an O-AGCM of the influence of variations of the solar constant on the global climate. Climate Dynam 13:757–767

Druffel ERM, Griffin S (1993) Large variations of surface ocean radiocarbon: evidence of circulation changes in the southwestern Pacific since 1657 AD. Paleoceanography 13:412–426

Eddy J (1976) The Late Maunder Minimum. Science 192:1189–1202

Esper J, Cook ER, Schweingruber FH (2002) Low-frequency signals in long tree-ring chronologies for reconstructing past temperature variability. Science 295:2250–2253

Feichter J, Kjellström E, Rodhe H, Dentener F, Lelieveld J, Roelofs GJ (1996) Simulation of the tropospheric sulfur cycle in a global climate model. Atmos Environ 30:1693–1707

Feichter J, Lohmann U, Schult I (1997) The atmospheric sulfur cycle and its impact on the shortwave radiation. Climate Dynam 13:235–246

Foukal P, North G, Wigley T (2004) A stellar view on solar variations and climate. Science 306:68–69

Glaser R (2001) Klimageschichte Mitteleuropas: 1000 Jahre Wetter, Klima, Katastrophen. Wiss. Buchgesellschaft Darmstadt

Glück MF, Stockton CW (2001) Reconstruction of the North Atlantic Oscillation, 1429–1983. Int J Clim 21:1453–1465

González-Rouco F, von Storch H, Zorita E (2003) Deep soil temperatures as proxy for surface air-temperatures in a coupled model simulation of the last thousand years. Geophys Res Lett 30. DOI 10.1029/2003GL018264

Govindasamy B, Duffy P, Caldera K (2001) Land use change and Northern Hemisphere cooling. Geophys Res Lett 28:291–294

Hagemann S, Botzet M, Dümenil L, Machenhauer B (1999) Derivation of global GCM boundary conditions from 1 km land use satellite data. MPI Report 289, Max-Planck-Institut für Meteorologie, Hamburg

Hansen J, Sato M, Nazarenko L, Ruedy R, Lacis A, Koch D, Tegen I, Hall T, Shindell D, Santer B, Stone P, Novakov T, Thomason L, Wang R, Wang Y, Jacob D, Hollandsworth S, Bishop L, Logan J, Thompson A, Stolarski R, Lean J, Willson R, Levitus S, Antonov J, Rayner N, Parker D, Christy J (2002) Climate forcings in Goddard Institute for Space Studies SI2000 simulations. J Geophys Res 107. DOI 10.1029/2001JD001143

Harington CR (ed) (1992) The year without a summer?—World climate in 1816. Canadian Museum of Nature, Ottawa, 576 pp

Hegerl GC, Hasselmann K, Cubasch U, Mitchell JFB, Roeckner E, Voss R, Waszkewitz J (1997) Multi-fingerprint detection and attribution analysis of greenhouse gas, greenhouse gas-plus-aerosol and solar forced climate. Climate Dynam 13:613–634

Hendy EJ, Gagan MK, Alibert CA, McCulloch MT, Lough JM, Isdale PJ (2002) Abrupt decrease in tropical Pacific sea surface salinity at the end of the Little Ice Age. Science 295:1511–1514

Huang SH, Pollack NH, Shen PY (2000) Temperature trends over the past five centuries reconstructed from borehole temperatures. Nature 403:756–758

IPCC (2001) Climate change 2001: the scientific basis. Cambridge University Press, Cambridge, 881 pp

Jones PD, Mann ME (2004) Climate over past millennia. Rev Geophys 42. DOI 2003RG00143

Klein Goldewijk K (2001) Estimating global land use change over the past 300 years: the HYDE database. Glob Biogeochem Cycl 15:415–433

Lamb HH (1970) Volcanic dust in the atmosphere; with a chronology and assessment of its meteorological significance. Philos Trans R Soc Lond A 266:425–533

Lamb HH (1982) Climate, history and the modern world. Methuen & Co, London

Latif M, Roeckner E, Mikolajewicz U, Voss R (2000) Tropical stabilization of the thermohaline circulation in a greenhouse warming simulation. J Climate 13:1809–1813

Lean J, Beer J, Bradley R (1995) Reconstruction of solar irradiance since 1610: implications for climate change. Geophys Res Lett 22:3195–3198

Lohmann U, Feichter J (1997) Impact of sulfate aerosols on albedo and lifetime of clouds: A sensitivity study with the ECHAM4 GCM. J Geophys Res 102:13685–13700

Lorenz S, Lohmann G (2004) Acceleration technique for Milankovitch type forcing in a coupled atmosphere-ocean circulation model: method and application for the Holocene. Climate Dynam 23:727–743

Luterbacher J (2001) The Late Maunder Minimum. In: Jones PD, Ogilvie AEJ, Davies TD, Briffa KR (eds) History and climate: memories of the future? Kluwer/Plenum, Dordrecht, New York, 295 pp

Luterbacher J, Rickli R, Xoplaki E, Tinguely C, Beck C, Pfister C, Wanner H (2001) The Late Maunder Minimum (1675–1715)—a key period for studying decadal scale climatic change in Europe. Clim Change 49:441–462

Luterbacher J, Xoplaki E, Dietrich D, Jones PD, Davies TD, Portis D, González-Rouco JF, von Storch H, Gyalistras D, Casty C, Wanner H (2002) Extending North Atlantic Oscillation records back to 1500. Atmos Sci Lett 20:114–124

Luterbacher J, Dietrich D, Xoplaki E, Grosjean M, Wanner H (2004) European seasonal and annual temperature variability, trends and extremes since 1500. Science 303:1499–1503

Manley G (1974) Central England temperatures: Monthly means 1659–1973. Q J R Met Soc 100:389–405

Mann ME, Bradley RS, Hughes MK (1998) Global-scale temperature patterns and climate forcing over the past six centuries. Nature 392:779–787 plus corrigendum (Mann ME, Bradley RS, Hughes MK (2004) Nature 430:105)

Mann ME, Bradley RS, Hughes MK (1999) Northern Hemisphere temperatures during the past millennium: Inferences, uncertainties and limitations. Geophys Res Lett 26:759–762

Mann ME, Jones PD (2003) Global surface temperature over the past two millennia. Geophys Res Lett 30. DOI 10.1029/2003GL017814

Matthews HD, Weaver AJ, Eby M, Meissner KJ (2003) Radiative forcing of climate by historical land cover change. Geophys Res Lett 30. DOI 10.1029/2002GL016098

Matthews HD, Weaver AJ, Meissner KJ, Gillett NP, Eby M (2004) Natural and anthropogenic climate change: incorporating historical land cover change, vegetation dynamics and the global carbon cycle. Climate Dynam 22:461–479

Moberg A, Sonechkin DM, Holmgren K, Datsenko NM, Karlén, W (2005) Highly variable Northern Hemisphere temperatures reconstructed from low- and high-resolution proxy data. Nature 433:613–617

Nakicenovic N, Alcamo J, Davis G, de Vries B, Fenhann J, Gaffin S, Gregory K, Grübler A, Jung TY, Kram T, La Rovere EL, Michaelis L, Mori S, Morita T, Pepper W, Pitcher H, Price L, Raihi K, Roehrl A, Rogner HH, Sankovski A, Schlesinger M, Shukla P, Smith S, Swart R, van Rooijen S, Victor N, Dadi Z (2000) IPCC special report on emissions scenarios. Cambridge University Press, Cambridge, 599 pp

Newhall C, Self S (1982) The volcanic explosivity index (VEI): an estimate of explosive magnitude for historical volcanism. J Geophys Res 87:1281–1283

Oberhuber JM (1993) Simulation of the Atlantic circulation with a coupled sea ice-mixed layer-isopycnal general circulation model. Part I: model description. J Phys Oceanogr 22:808–829

Pfister C (1999) Wetternachhersage. 500 Jahre Klimavariationen und Naturkatastrophen 1496-1995. Haupt Verlag, Bern

Quinn TM, Crowley TJ, Taylor FW, Henin C, Joannot P, Join Y (1998) A multicentury isotopic record from a New Caledonia coral: Interannual and decadal sea surface temperature variability in the southwest Pacific since 1657 A.D. Paleoceanography 13:412–426

Rahmstorf S, Ganopolsky A (1999) Long-term global warming scenarios computed with an efficient coupled climate model. Clim Change 43:353–367

Ramaswamy V, Schwarzkopf MD, Randel WJ (1996) Fingerprint of ozone depletion in the spatial and temporal pattern of recent lower-stratospheric cooling. Nature 382:616–618

Robertson A, Overpeck J, Rind D, Mosley-Thompson E, Zielinski G, Lean J, Koch D, Penner J, Tegen I, Healy R (2001) Hypothesized climate forcing time series for the last 500 years. J Geophys Res 106:14783–14803

Robock A (1994) Review of the year without a summer. World Climate in 1816. Clim Change 26:105–108

Robock A (2000) Volcanic eruptions and climate. Rev Geophys 38:191–220

Robock A, Free MP (1995) Ice cores as an index of global volcanism from 1850 to the present. J Geophys Res 100:11549–11567

Robock A, Free MP (1996) The volcanic record in ice cores for the past 2000 years. In: Jones PD, Bradley RS, Jouzel J (eds): Climatic variations and forcing mechanisms of the last 2000 years. Springer, Berlin Heidelberg New York, pp 533–546

Robock A, Mao J (1995) The volcanic signal in surface temperature observations. J Climate 8:1086–1103

Roeckner E, Bengtsson L, Feichter J, Lelieveld J, Rodhe H (1999) Transient climate change simulations with a coupled atmosphere-ocean GCM including the tropospheric sulfur cycle. J Climate 12:3004–3032

Roelofs GJ, Lelieveld J (1995) Distribution and budget of O_3 in the troposphere calculated with a chemistry-general circulation model. J Geophys Res 100:20983–20998

Sato M, Hansen J, McCormick M, Pollack J (1993) Stratospheric aerosol optical depth, 1880–1990. J Geophys Res 98:22987–22994

Schmutz C, Luterbacher J, Gyalistras D, Xoplaki E, Wanner H (2000) Can we trust proxy-based NAO index reconstructions? Geophys Res Lett 27:1135–1138

Self S, Gertisser R, Thordarson T, Rampino MR, Wolff JA (2004) Magma volume, volatile emissions and stratospheric aerosols from the 1815 eruption of Tambora. Geophys Res Lett 31. DOI 10.1029/2004GL020925

Shindell DT, Schmidt GA, Mann ME, Rind D, Waple A (2001a) Solar forcing of regional climate change during the Maunder Minimum. Science 294:2149–2152

Shindell DT, Schmidt GA, Miller RL, Rind D (2001b) Northern Hemisphere winter climate response to greenhouse gas, ozone, solar and volcanic forcing. J Geophys Res 106:7193–7210

Solanki SK, Usoskin IG, Kromer B, Schussler M, Beer J (2004) Unusual activity of the Sun during recent decades compared to the previous 11000 years. Nature 431:1084–1087

Stendel M, Schmith T, Roeckner E, Cubasch U (2000) The climate of the 21st century: Transient simulations with a coupled atmosphere-ocean general circulation model. Danish Met Inst Report 02-1, 51 pp

von Storch H, Zorita E, Jones JM, Dimitriev Y, González-Rouco F, Tett SFB (2004) Reconstructing past climate from noisy data. Science 306:679–682

Stothers RB (1984) The great Tambora eruption in 1815 and its aftermath. Science 224:1191–1198

Stothers RB (2001) Major optical depth perturbations to the stratosphere from volcanic eruptions: Stellar extinction period, 1961–1978. J Geophys Res 106:2993–3004

Stott PA, Tett SFB, Jones GS, Allen MR, Mitchell JFB, Jenkins GJ (2000) External control of 20th century temperature variations by natural and anthropogenic forcings. Science 290:2133–2137

Tibaldi S, Tosi E, Navarra A, Pedulli E (1994) Northern and Southern Hemisphere seasonal variability of blocking frequency and predictability. Mon Wea Rev 122:1971–2003

Vinther BM, Johnsen SJ, Andersen KK, Clausen HB, Hansen AW, 2003: NAO signal recorded in the stable isotopes of Greenland ice cores. Geophys Res Lett 30. DOI 10.1029/2002GL016193

Xoplaki E, Maheras P, Luterbacher J (2001) Variability of climate in meridional Balkans during the periods 1675–1715 and 1780–1830 and its impact on human life. Clim Change 48:581–614

Zhao M, Pitman A, Chase T (2001) The impact of land cover change on the atmospheric circulation. Climate Dynam 17:467–477

Zorita E, von Storch H, Gonzalez-Rouco FJ, Cubasch U, Luterbacher J, Legutke S, Fischer-Bruns I, Schlese U (2004) Simulation of the climate of the last five centuries. Met Z 13:271–289